

Article

Barkhausen Noise Assessment of the Surface Conditions Due to Deep Hole Drilling and Their Influence on the Fatigue Behaviour of AISI 4140

Nikolas Baak ^{1,*} , Fabian Schaldach ¹, Jan Nickel ², Dirk Biermann ² and Frank Walther ¹

¹ Department of Materials Test Engineering (WPT), TU Dortmund University, Baroper Str. 303, D-44227 Dortmund, Germany; Fabian.Schaldach@tu-dortmund.de (F.S.); frank.walther@tu-dortmund.de (F.W.)

² Institute of Machining Technology (ISF), TU Dortmund University, Baroper Str. 303, D-44227 Dortmund, Germany; Nickel@isf.de (J.N.); Biermann@isf.de (D.B.)

* Correspondence: Nikolas.Baak@tu-dortmund.de; Tel.: +49-231-755-8410

Received: 21 August 2018; Accepted: 11 September 2018; Published: 13 September 2018



Abstract: In many technical fields, high-strength steels like AISI 4140 are commonly used for highly dynamically loaded parts. Increasing demands on weight, performance and efficiency of the automotive industry lead to increasing demands on material properties. For surface conditioning, optimised machining processes are capable of improving the fatigue performance without increasing the production cost significantly. This paper compares the influence of three different sulphur contents and three different feed rates on the fatigue behaviour of deep hole drilled AISI 4140 fatigue specimens. The specimens were characterised regarding their surface condition, hardness and microstructure, and afterwards they were tested under fatigue loading for performance assessment. These tests were accompanied with Barkhausen noise analysis. The Barkhausen noise signal was detected by a custom-built sensor that is capable of detecting the magnetic values on the bore wall. Using this technique, a load-independent estimation of fatigue damage was established.

Keywords: structural health monitoring; fatigue behaviour; quenched and tempered steel; AISI 4140; 42CrMo4 + QT; surface condition; magnetic Barkhausen noise

1. Introduction

Quenched and tempered steels like AISI 4140 (42CrMo4 + QT) are often used for highly loaded parts in plant engineering or engine components. These parts are regularly processed via machining operations like deep drilling. Typical examples for deep drilled engine components are rails of fuel injection systems [1]. These rails are loaded with a severe internal pressure of up to 2500 bar, and, for the aim of increasing power output by lower fuel consumption, the pressure should be increased up to 3000 bar [2]. To withstand these increasing loads, either optimised materials or manufacturing methods have to be developed. Currently, autofrettage is a common process to enhance the fatigue life of the deep hole drilled rails [3]. The process induces residual stresses in the inner part surface by an inner pressure exceeding the operational load. Plastic deformations at the inner surface in combination with elastic deformations lead to compressive residual stresses at the crucial inner surface [4]. This process is very cost- and time-intensive, and the effort even increases with a smaller diameter and higher depth of the bore [5,6]. An optimisation of the applied material can be another approach to fulfil the increasing demands. The purity of the alloy, especially the sulphur content, has a major influence on the service life of fatigue-loaded parts [7]. The downsides of lower sulphur content are worse drilling properties, since the manganese sulphides improve the chip breaking.

This work investigates the possibility to induce residual stresses in the bore wall by an optimised drilling process with the aim to avoid expensive post-processing steps. The asymmetrical design of a single lip deep drilling tool, which supports the drilling forces via guide pads on the bore wall leads, on the one hand, to good surface finish and, on the other hand, to a mechanical influence of the surface layer [8]. It offers good possibilities to pare down the autofrettage step. Besides the maximum value of the stresses, the redistribution and the stability under fatigue load are highly relevant [9]. Holzapfel et al. showed that the residual stresses relax due to fatigue loading [10].

The process was evaluated on three melts of AISI 4140 with varying sulphur content to characterise the conflicting influence of sulphur on the fatigue performance and the machinability. The non-destructive characterisation of the microstructure and residual stresses is impossible by conventional methods, so the resulting crucial surface layer was characterised by micromagnetic methods using a custom-made inner-surface sensor. The determination of the micromagnetic properties and their development during fatigue loading offer a wide range of correlations to mechanical properties like hardness, residual stresses and technological parameters [11–14].

2. Materials and Methods

In this work, three melts of AISI 4140 with sulphur content of 0.0076 wt % (S76), 0.0110 wt % (S110) and 0.0280 wt % (S280) are evaluated. Table 1 shows the chemical compositions. Except for sulphur, no significant differences in chemical compositions are noticeable. All materials comply the limits in chemical composition for 42CrMo4 and 42CrMoS4, respectively, defined in EN 10083-3.

Table 1. Chemical compositions (wt %).

Melts	C	Si	Mn	P	S	Cr	Mo	Fe
S76	0.41	0.33	0.66	0.009	0.008	0.96	0.16	bal.
S110	0.41	0.18	0.85	0.011	0.011	1.01	0.18	bal.
S280	0.39	0.17	0.83	0.014	0.028	0.97	0.17	bal.

The number, size and shape of the manganese sulphides are mainly influenced by the sulphur content. Figure 1 shows the manganese sulphide distribution for all alloys on polished microsections in the rolling direction. It can be noticed that the manganese sulphides are elongated in the direction of rolling and that the inclusion size increases with the sulphur content.

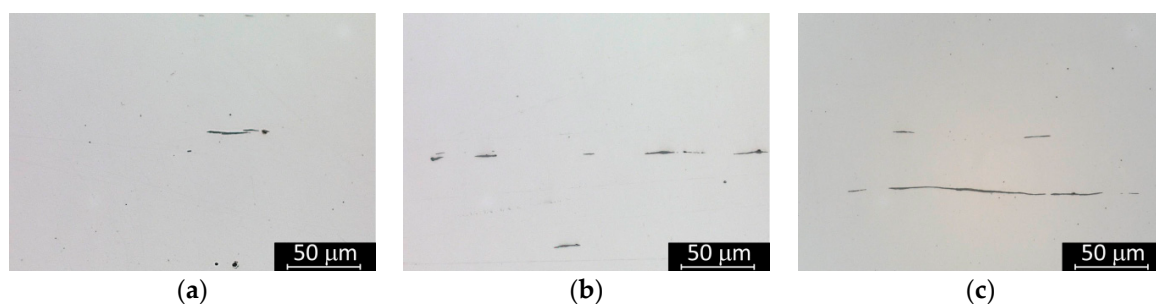


Figure 1. Polished microsections for the alloys (a) S76; (b) S110; (c) S280.

In the present case, all alloys show quenched and tempered microstructure with comparable characteristics. Figure 2 shows etched microsections from the centre of the bulk material.

Single-lip deep hole drilling is characterised by excellent results with regard to the quality of the bore in terms of surface roughness and straightness deviation, as well as roundness and radial deviation. Due to its asymmetrical design, the single-lip drill is equipped with guide pads, which, on the one hand, allow the tool to guide itself in the bore, but also transmit the cutting and passive forces that occur during the process into the bore wall [15]. This smoothed the surface of the bore

and at the same time influences the subsurface area by initiating changes in the microstructure and inducing residual stresses. The resulting surface integrity can be influenced by adjusting the process parameters' cutting speed and feed rate. The geometry of the drilling tools is another aspect that has an influence on the occurring forces during the machining process which affects the bore surface and subsurface [16].

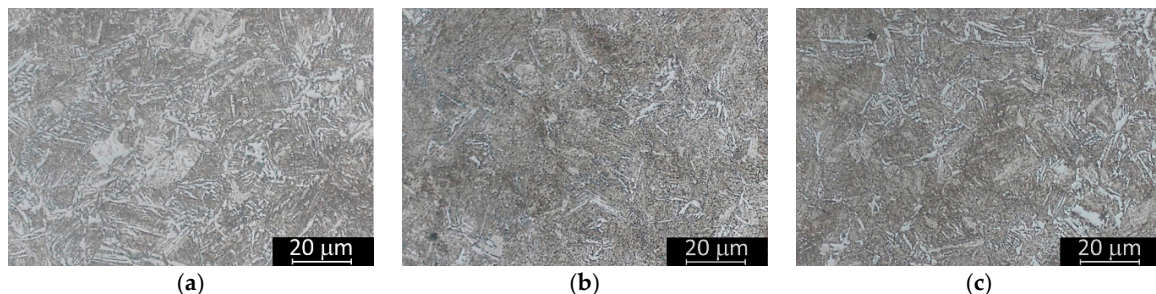


Figure 2. Etched microsections for the alloys (a) S76; (b) S110; (c) S280.

In a first step, circumferential shape of the tool, the geometry of the guide rails as well as the guide rail coatings were varied. Based on feed force and torque during the drilling process, hardness measurements and microstructural investigations on transverse microsections, a tool was selected.

Afterwards, the bulk material was deep hole drilled by a constant cutting speed of $v_c = 65$ m/min with three different feed rates, a high feed rate $f = 0.15$ mm, an intermediate rate $f = 0.10$ mm and a low rate $f = 0.05$ mm. From these deep hole drilled bulk material, fatigue specimens according to Figure 3b were produced. Thus, nine sample variants were available for further investigations.

The magnetic Barkhausen noise (MBN) is based on unsteady changes in the areal expansion of magnetic domains in ferromagnetic materials. The Weiss domains are divided by Bloch walls, which move when an external magnetisation occurs. The movement is affected by lattice distortions, like inclusions or dislocations, and the magnetostriction. In a constantly changing magnetic field, a characteristic in the Bloch wall movement can be observed and traced back to the microstructure and residual stresses. Jiles showed that increasing the compressive stresses leads to an increase in coercive field strength and a decrease in the maximum of the Barkhausen noise amplitude [17]. The skin effect causes a maximum penetration depth for the MBN signal of approximately $100 \mu\text{m}$, thus it is important to detect the MBN on the crucial surface [18]. Therefore, the micromagnetic properties were tested with a custom-built inner surface Barkhausen noise sensor designed for the "FracDim" measuring device (Fraunhofer IKTS, Dresden, Germany) as shown in Figure 3a. With this unique sensor, the characterisation of the residual stresses induced by the drilling process can be non-destructively realised on the inner specimen surface. To quantify the induced residual stresses and to validate the MBN measurements, X-ray diffraction (XRD) investigations were performed on bore surfaces.

Moreover, the specimens were characterised concerning their microhardness, microstructure and roughness. The results were correlated with the outcomes of the mechanical investigations to show the dependence of the fatigue life on the surface layer condition. Roughness measurements and microstructure were carried out on S110 specimens for all feed rates. A MarSurf XR 20 (Mahr, Göttingen, Germany) was used for surface characterisation. Microhardness mappings were performed with a HMV-G (Shimadzu, Kyoto, Japan) on transverse microsections of unloaded specimens. The microstructural investigations were done with a Axio Imager.M1m light microscope (Zeiss, Göttingen, Germany) and a Mira3 scanning electron microscope (Tescan, Brno, Czech Republic).

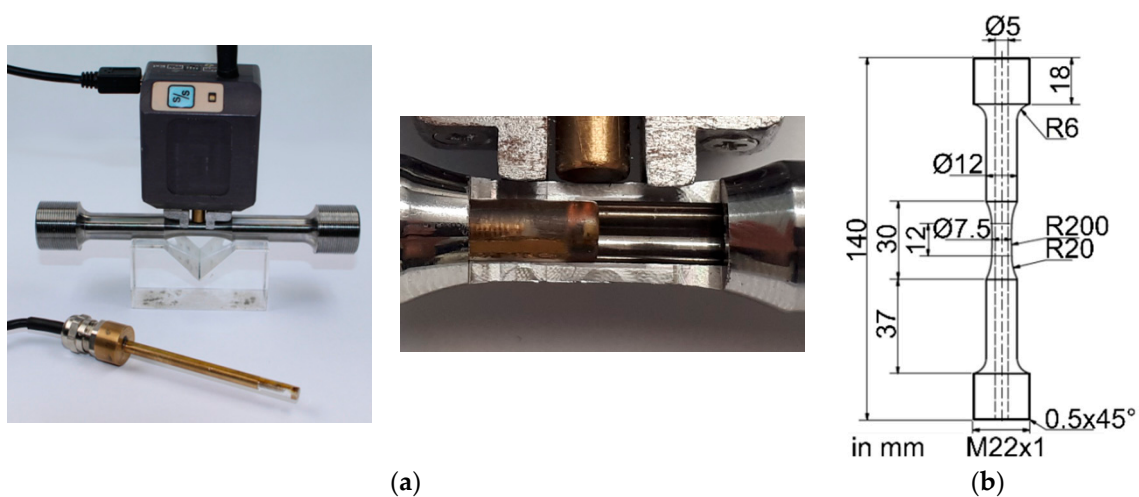


Figure 3. (a) custom-built inner surface sensor; (b) technical drawing of the deep hole drilled fatigue specimen (dimensions in mm).

Load increase tests (LIT) and constant amplitude tests (CAT) were carried out with a Testronic 150 kN resonant testing system (Russenberger Prüfmaschinen AG, Neuhausen am Rheinfall, Switzerland). The tests were performed with a frequency of ~ 75 Hz and a stress ratio of $R = -1$ (fully-reversed loading). The LIT started at a damage-free amplitude of $\sigma_a = 100$ MPa and was increased by $\Delta\sigma_a = 10$ MPa each $\Delta N = 10^4$ load cycles. To detect first microstructural changes, the specimens were instrumented with a tactile extensometer, an alternating current potential drop (ACPD) set-up and thermocouples (Figure 4). These measurement devices allow the detection of first plastic deformations during fatigue loading. Plastic deformations and therefore first damages are indicated during LIT as the change from linear to exponential slope in measured values [19].

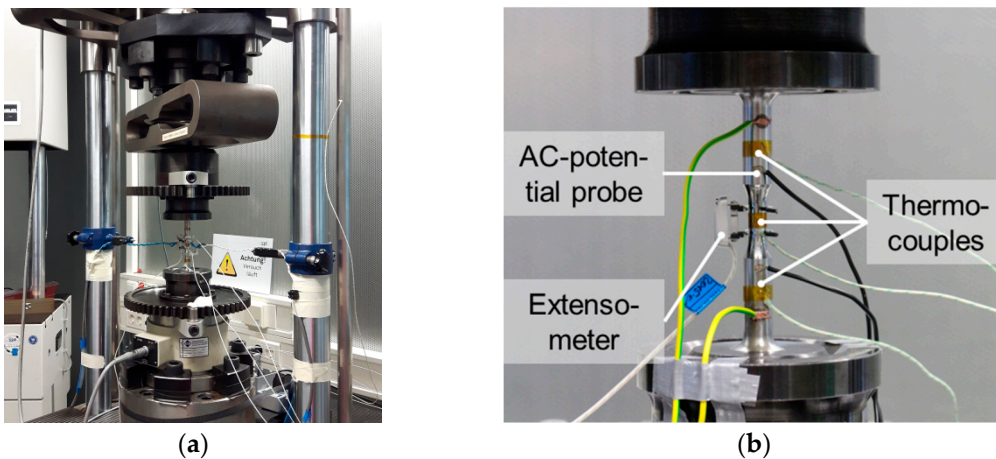


Figure 4. (a) Rumul Testronic 150 kN; (b) instrumented fatigue specimen applied in the testing system.

Instrumented LIT were performed to estimate the fatigue strength and to identify suitable amplitudes for CAT, which were carried out for most promising material S110 in LIT and three feed rates. The CAT tests were interrupted for MBN measurements to investigate the development of residual stresses on the inner surface of the bore. Moreover, the evolving deformation-induced relaxation process can be characterised.

3. Results

3.1. Tool Design

In a series of machining tests, eight variants of single-lip drills with different cutting edge grindings, circumferential shapes and coatings were used and the feed forces and the drilling torque were measured (Figure 5). The tool grinding significantly influences the measured force and torque during the single-lip deep hole drilling process. It turned out that, when using a tool with a significantly larger external cutting edge, the drilling torque was about 40% higher (variant 8) than with a tool with a standard faceted ground edge (variant 6). With faceted grinding, the inner and outer cutting edge are approximately of the same length so a passive force equilibrium between the inner and outer cutting edge is achieved. On tools with radius grinding, the outer cutting edge is considerably larger than the inner cutting edge. This has an effect on the ratio of passive forces so the tool is pushed towards its centre. Because the tool is guided at the wall of the bore via the guide pads, the higher passive forces lead to an increase of the normal force, which presses the guide pads against the bore wall. As a result, the measured drilling torque increases as well. The effects on the bores surface layer were analysed by microhardness measurements on cross-sections of the drilled specimens. The hardness at the bore subsurface when using tools with a larger outer cutting edge was considerably higher than with standard ground tools.

The variation of the circumferential shapes G, with a continuous guide rail, and A, with three narrow guide rails, showed no significant differences in feed force or drilling torque. However, the hardening in the surface layer of the bores was lower with the circumferential form G. This can be explained by the higher surface pressure as a result of the narrow guide rails. Due to the higher surface pressure, the surface of the bore is more smoothened, the microstructure of the surface layer is more refined and hardened by the higher normal forces and presumably also higher residual stresses are introduced into the bore wall [20,21]. The variation between AlTiN and TiN coating of the tools showed no significant differences in the height of the feed forces and moments. The obtained results were taken into account for selecting tool variant 8 as the reference tool for the subsequent test, as the higher mechanical load and the high surface pressure are expected to strengthen the bore surface. The resulting mechanical hardening of the surface layer and induction of residual stresses is supposed to increase the fatigue strength.

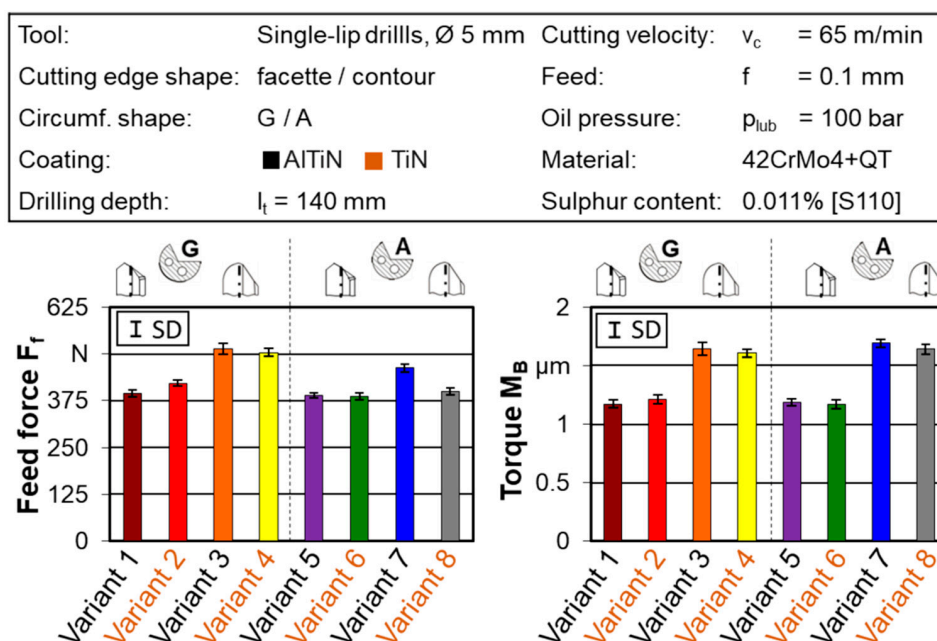


Figure 5. Measured feed force and torque using different drill variants [22].

3.2. Characterisation of the Surface Layer

The metallographic investigations on etched transverse microsections, displayed in Figure 6, reveal a white etching layer (WEL) with a maximum thickness of approx. 6 μm on the surface of the bore. It can be seen that the sulphur content and the feed rate promote the formation of a WEL. This is reflected in thicker WEL for S280 in comparison with S110 and its absence for S76. The influence of the feed rate manifests itself in an increasing layer thickness for higher feed rates in S110 and S280.

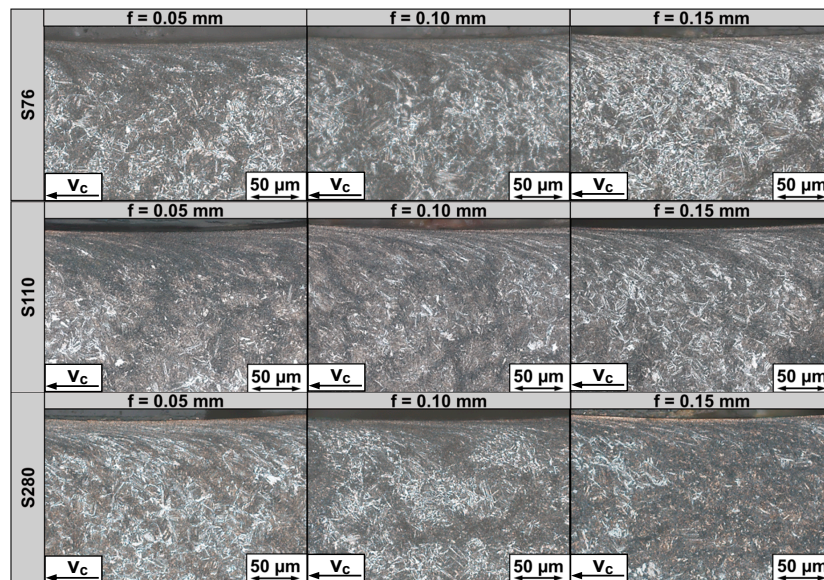


Figure 6. Microstructure of specimens made of S76, S110 and S280 and feed rates 0.05 mm, 0.10 mm and 0.15 mm.

Scanning electron microscopic investigations (Figure 7) allow a more detailed examination of influenced surface layer. These investigations reveal that the thickness of the surface layer in S110 for $f = 0.05 \text{ mm}$ and 0.10 mm are comparable, whereas the thickness of the layer for $f = 0.15 \text{ mm}$ is significantly thinner.

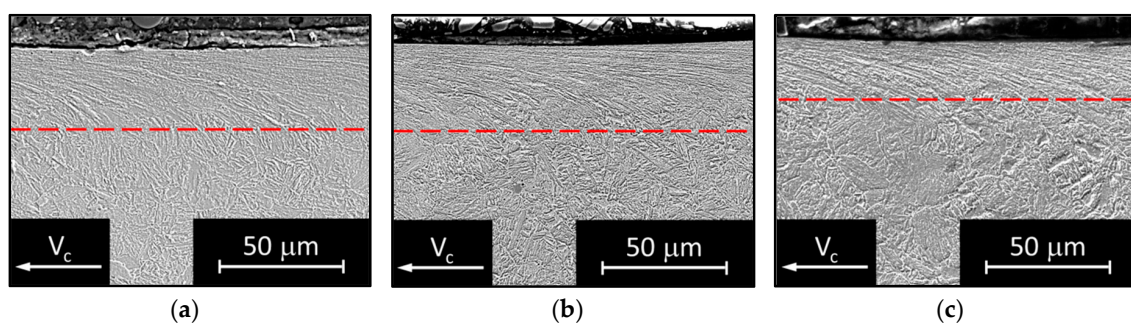


Figure 7. Scanning electron micrographs of S110 specimen with a feed rate of (a) 0.05 mm; (b) 0.10 mm; (c) 0.15 mm.

The surface quality of S110 specimens was examined by tactile roughness measurements. Table 2 displays the results in tabular form. The feed rate has no significant influence on the surface roughness.

Table 2. Results of tactile roughness measurements on S110 specimens.

S110			
f (mm)	0.05	0.10	0.15
R _a (μm)	0.24	0.29	0.23
R _z (μm)	2.07	2.12	2.07

Microhardness mappings on S110 (Figure 8) show that feed rate $f = 0.05$ mm (a) leads to the highest hardness increase in the surface layer from 250 HV 0.01 to about 440 HV 0.01. For higher feed rates of 0.10 mm, (b) a lower increase to 410 HV 0.01 and for 0.15 mm (c) to 380 HV 0.01 can be detected. The mostly pronounced hardness layer can be found for a feed rate of $f = 0.10$ mm.

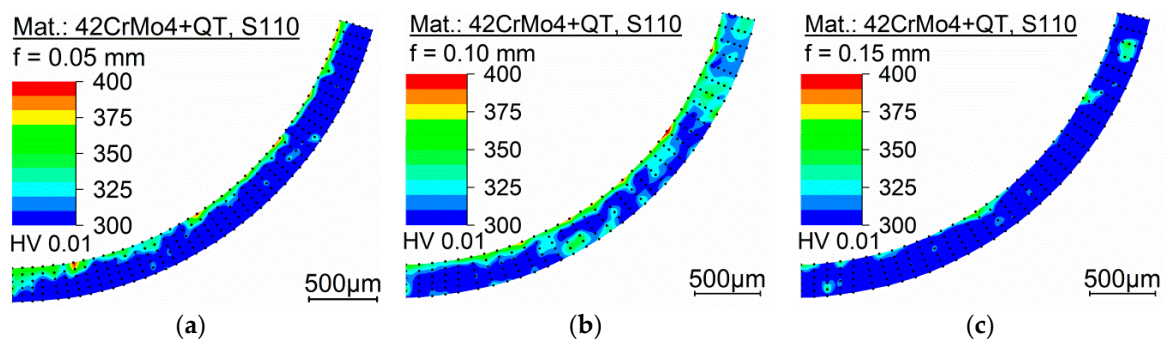


Figure 8. Microhardness mappings (HV0.01) of deep drilled S110 specimen with varying feed rate of (a) 0.05 mm; (b) 0.10 mm; (c) 0.15 mm.

XRD measurements on the inner surface of the bore were performed for the initial state. It was found that all feed rates induce residual stresses in the surface layer (Figure 9a). The characteristic profile of the stresses does not vary significantly with the feed rates investigated. However, the integral width (Figure 9b), which is an indicator for lattice distortion density and therefore residual stresses of type III and work hardening [23,24], is higher for the feed rate $f = 0.10$ mm in comparison to the others.

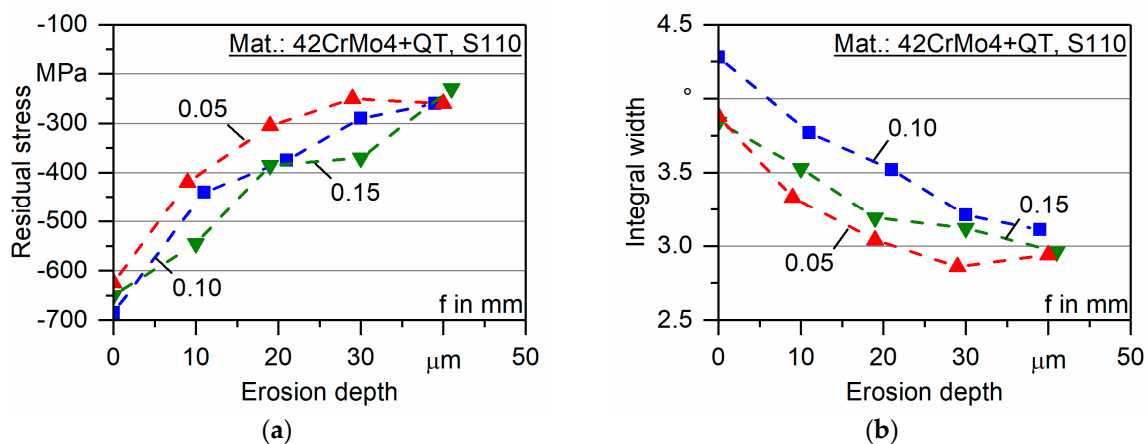


Figure 9. Results of XRD measurements of S110 specimen drilled with varying feed rate (a) residual stresses; (b) integral width.

The characterisation of the surface layer in the initial state showed that the feed rate of 0.10 mm leads to the highest mechanical influences in the bore wall. The increase from 0.05 mm to 0.10 mm can be explained by higher process forces. A further increase to 0.15 mm may lead to a critical temperature increase which promotes the chip formation and, therefore, inhibits further mechanical influences of the surface layer [25].

3.3. Fatigue Tests

The LIT results (Table 3) show that S110 leads to the highest failure stress amplitudes, whereas the feed rate shows no significant influence on $\sigma_{a,f}$. In Figure 10a, the material reaction of S110 with $f = 0.10$ mm during the LIT is presented, and the change in plastic strain amplitude indicates first fatigue-induced material reactions from $\sigma_a = 450$ MPa. The specimens' self-heating, caused by the increasing plastic deformations, leads to a temperature increase of about 3 K at $\sigma_a = 450$ MPa. Therefore, an influence of the temperature increase on the fatigue strength estimation is not expected. In Figure 10b, a comparison of the plastic strain amplitude $\epsilon_{a,p}$ is plotted versus the number of cycles N for S110 and all feed rates from 0.05 to 0.15 mm. The material reaction of the S110 specimen with $f = 0.10$ mm starts at a slightly higher amplitude of $\sigma_a = 450$ MPa compared to $\sigma_a = 420$ MPa for $f = 0.15$ mm and $\sigma_a = 400$ MPa for $f = 0.05$ mm.

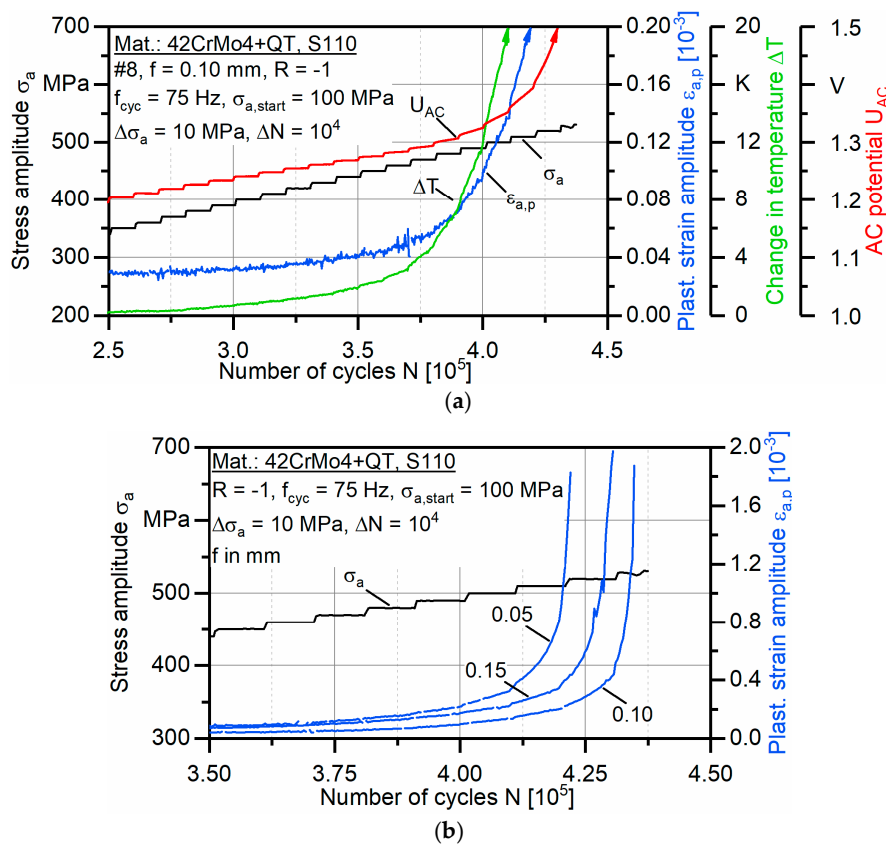


Figure 10. (a) Load increase tests on S110 specimen and feed rate 0.10 mm; (b) comparison of plastic strain amplitude during load increase tests on S110 specimens and feed rates from 0.05 to 0.15 mm. Data from [26].

Table 3. Results of load increase tests on 42CrMo4 + QT.

Melt	S76			S110			S280		
f (mm)	0.05	0.10	0.15	0.05	0.10	0.15	0.05	0.10	0.15
$\sigma_{a,f}$ (MPa)	470	470	470	520	530	530	510	500	520

Afterwards, CAT with stress amplitudes between 400 and 500 MPa were performed for S110 specimens and all feed rates. The results are concluded in a Woehler diagram (Figure 11) showing that the feed rates 0.05 mm and 0.15 mm lead to comparable fatigue behaviour. Feed rate 0.10 mm leads to a smaller slope of Basquin curve, which results in inferior performance for higher amplitudes, but to a higher fatigue limit.

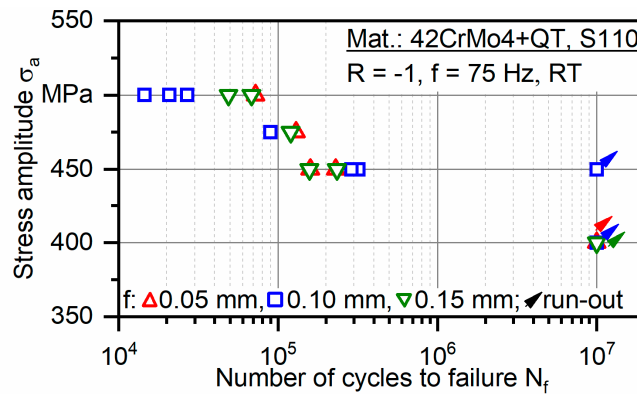
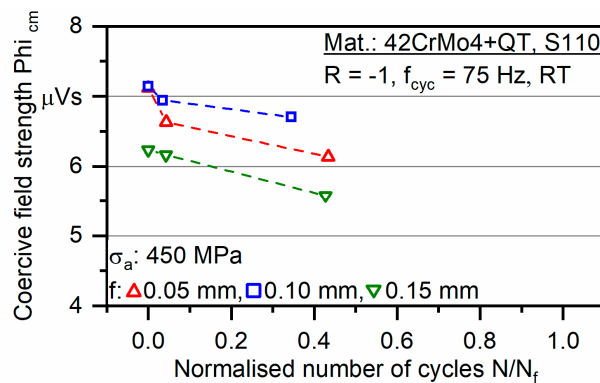


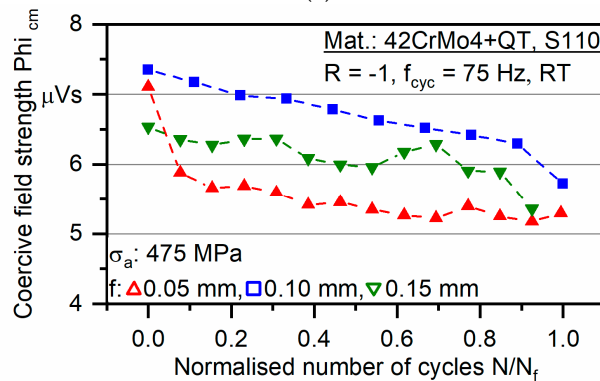
Figure 11. Woehler diagram for S110 specimens and feed rates from 0.05 to 0.15 mm.

A decrease in the slope of the Basquin curve was shown for autofrettaged specimen compared to a non-autofrettaged specimen by Thumser et al. [3], leading to the assumption that the feed rate $f = 0.10$ mm results could be comparable to that of autofrettaged specimens.

The CAT for $\sigma_a = 450$ MPa (Figure 12a) and 475 MPa (Figure 12b) were interrupted for micromagnetic measurements. The 450 MPa tests were interrupted at 0, 10^4 and 10^5 cycles. The specimen of the 475 MPa test was measured at 0 cycles and every following 10^4 cycles. The coercive field strength Φ_{cm} is plotted against the normalised number of cycles N/N_f . For some feed rates and load amplitudes, Φ_{cm} drops significantly during the first 10^4 cycles. Afterwards, Φ_{cm} decreases steadily with proceeding fatigue damage.



(a)



(b)

Figure 12. Coercive field strength versus the normalised number of cycles for constant amplitude tests with S110 specimens and amplitudes (a) 450 MPa; (b) 475 MPa.

When the coercive field strength is also normalised on the 10^4 cycles value, a quadratic relationship between the coercive field strength and the proceeding fatigue damage can be observed for all investigated load amplitudes and all feed rates, whereby the best correspondence can be seen for the feed rates 0.05 mm and 0.10 mm. This relationship can be described with the following Equation (1):

$$\frac{\Phi_{cm}}{\Phi_{cm, 10^4}} = 1 - 0.174 \frac{N}{N_f} + 0.048 \left(\frac{N}{N_f} \right)^2. \quad (1)$$

The decreasing coercive field strength can be correlated to relaxing compressive residual stresses. The stresses decrease according to the magnitude of the initial stresses and the applied load [10]. In consideration of the XRD measurements of the initial state, the specimen condition after first applied load cycles is much more significant than the initial state. Moreover, the normalisation of the coercive field strength Φ_{cm} as a micromagnetic parameter and the number of cycles as lifetime state allows a load- and material-independent estimation of the fatigue damage (Figure 13).

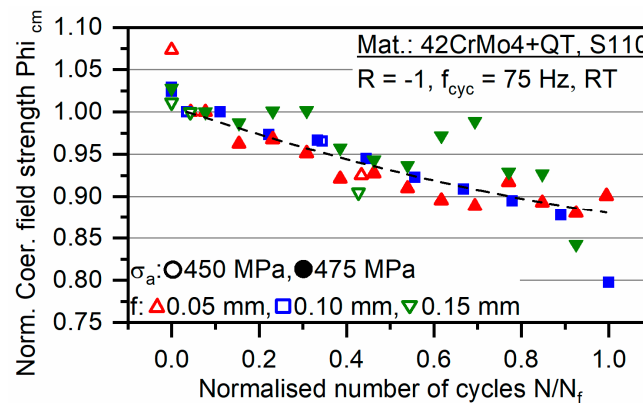


Figure 13. Normalised coercive field strength versus the normalised number of cycles for constant amplitude tests with S110 specimens and amplitudes of 450 MPa and 475 MPa.

4. Discussion and Conclusions

The material and drilling parameters have a significant influence on the fatigue performance. Contrary to the expectations, the alloy with the lowest sulphur content (S76) leads to the poorest fatigue performance; S110 and S280 result in comparable failure stress amplitudes in load increase tests. The investigation on the variation of the feed rate reveals that the intermediate feed rate 0.10 mm has the most significant impact on the surface layer. In particular, the hardening depth and the integral width show substantial differences. It can be assumed that the feed rate of 0.10 mm leads to the highest dislocation density with accompanied work hardening, whereas the induced residual stresses are on a comparable level. The constant amplitude tests showed that the influence of the drilling process impacts mainly the slope of the Basquin curve. This leads to higher fatigue strength of S110 specimens drilled with 0.10 mm and better performance of S110 specimens drilled with 0.05 mm and 0.15 mm for higher load amplitudes. This behaviour can also be seen in the load increase tests. The plastic strain amplitude in the S110 specimen drilled with 0.10 mm remains constant for low load steps and increases rapidly when critical load step is reached. The plastic strain amplitude increase for other feed rates is more continuous, leading to the assumption that the fatigue performance resulting from the intermediate feed rate could be comparable to that of autofrettaged specimens. The micromagnetic investigations offered the possibility of a fatigue life description with a quadratic function, independent of material condition and load, whereas the coercive field strength shows a significant drop from the initial state to 10^4 cycles. This singularity can be explained by stress degradation during the first load cycles.

The upcoming research should focus on the material response during the first 10^4 cycles and, accordingly, the change in coercive field strength and the progression of the residual stresses during fatigue life. With this examination, a separation of the effects by the fatigue load should be possible; in particular, the degradation of residual stresses is expected to be the main influence on the fatigue performance. Moreover, a fractographic investigation regarding the crack origin should be performed.

Author Contributions: J.N. provided the bulk material and performed the drilling experiments. N.B., F.S. and J.N. characterised the microstructure of the bulk material and the initial state. Fatigue tests, as well as characterisation methods of the surface layer during the tests, were performed by N.B. and F.S. The figures were prepared by N.B., F.S. and J.N. The original draft was written by N.B., F.W. and D.B. supervised the project and reviewed the manuscript.

Funding: The authors thank the Deutsche Forschungsgemeinschaft (DFG, German Research Foundation) for its financial support within the research project 'Investigations on the influence of machining and sulphur content on the fatigue strength of the quenched and tempered steel 42CrMo4 + QT' (WA 1672/22-1, BI 493/83-1).

Acknowledgments: We acknowledge financial support by Deutsche Forschungsgemeinschaft (DFG, German Research Foundation) and TU Dortmund University within the funding programme Open Access Publishing.

Conflicts of Interest: The authors declare no conflict of interest.

References

1. Vormwald, M.; Schlitzer, T.; Panic, D.; Beier, H. Fatigue strength of autofrettaged diesel injection system components under elevated temperature. *Int. J. Fatigue* **2018**, *113*, 428–437. [[CrossRef](#)]
2. Hammer, J.; Raff, M.; Naber, D. Advanced diesel fuel injection equipment—A never ending Bosch story. In Proceedings of the 14th Internationales Stuttgarter Symposium, Stuttgart, Germany, 18–19 March 2014; Bargende, M., Reuss, H.C., Wiedemann, J., Eds.; Springer: Wiesbaden, Germany, 2014.
3. Thumser, R.; Bergmann, J.W.; Herz, E.; Hertel, O.; Vormwald, M. Variable amplitude fatigue of autofrettaged diesel injection parts. *Materialwiss. Werkstofftech.* **2008**, *39*, 719–725. [[CrossRef](#)]
4. Greuling, S.; Seeger, T.; Vormwald, M. Autofrettage innendruckbelasteter Bauteile. *Materialwiss. Werkstofftech.* **2006**, *37*, 233–239. [[CrossRef](#)]
5. Malik, A.; Kushnood, S. A review of swage-autofrettage process. In Proceedings of the 11th International Conference on Nuclear Engineering, Tokyo, Japan, 20–23 April 2003; The Japan Society of Mechanical Engineers: Tokyo, Japan, 2003.
6. Leutwein, H. *Einfluss von Autofrettage auf die Schwingfestigkeit Innendruckbelasteter Bauteile aus Kugelgraphitguss*, 2nd ed.; Ilmedia: Ilmenau, Germany, 2011; ISBN 978-3-939473-35-0.
7. Lei, Z.; Hong, Y.; Xie, J.; Sun, C.; Zhao, A. Effects of inclusion size and location on very-high-cycle fatigue behavior for high strength steels. *Mater. Sci. Eng. A-Struct.* **2012**, *558*, 234–241. [[CrossRef](#)]
8. Heilmann, M. Tiefbohren Mit Kleinen Durchmessern Durch Mechanische und Thermische Verfahren. Ph.D. Thesis, TU Dortmund, Dortmund, Germany, 2012.
9. Webster, G.A.; Ezeilo, A.N. Residual stress distributions and their influence on fatigue lifetimes. *Int. J. Fatigue* **2001**, *23*, 375–383. [[CrossRef](#)]
10. Holzapfel, H.; Schulze, V.; Vöhringer, O.; Macherauch, E. Residual stress relaxation in an AISI 4140 steel due to quasistatic and cyclic loading at higher temperatures. *Mater. Sci. Eng. A-Struct.* **1998**, *248*, 9–18. [[CrossRef](#)]
11. Moorthy, V.; Shaw, B.A.; Hopkins, P. Surface and subsurface stress evaluation in case-carburised steel using high and low frequency magnetic Barkhausen emission measurements. *J. Magn. Magn. Mater.* **2006**, *229*, 362–375. [[CrossRef](#)]
12. Santa-aho, S.; Vippola, M.; Sorsa, A.; Leiviskä, K.; Lindgren, M.; Lepistö, T. Utilization of Barkhausen noise magnetizing sweeps for case-depth detection from hardened steel. *NDT&E Int.* **2012**, *52*, 95–102. [[CrossRef](#)]
13. Baak, N.; Garlich, M.; Schmiedt, A.; Bambach, M.; Walther, F. Characterization of residual stresses in austenitic disc springs induced by martensite formation during incremental forming using micromagnetic methods. *Mater. Test.* **2017**, *59*, 309–314. [[CrossRef](#)]

14. Baak, N.; Tenkamp, J.; Walther, F.; Garlich, M.; Bambach, M.; Weibring, M.; Tenberge, P. Magnetische-Barkhausen-Rauschen-Analyse zur zerstörungsfreien Produktions- und Betriebsüberwachung lokaler physikalischer Eigenschaften. In Proceedings of the Werkstoffprüfung 2017–Fortschritte in der Werkstoffprüfung für Forschung und Praxis, Berlin, Germany, 30 November–1 December 2017; Frenz, H., Langer, J.B., Eds.; Stahleisen: Düsseldorf, Germany, 2017; pp. 129–134.
15. *Deep-Hole Drilling*; VDI Guideline 3210; Beuth Verlag: Berlin, Germany, 2006.
16. Sakuma, K.; Taguchi, K.; Katsuki, A.; Takeyama, H. Self-guiding action of deep-hole-drilling tools. *CIRP Ann.* **1981**, *30*, 311–315. [[CrossRef](#)]
17. Jiles, D.C. The effect of stress on magnetic Barkhausen activity in ferromagnetic steels. *IEEE Trans. Magn.* **1989**, *25*, 3455–3457. [[CrossRef](#)]
18. Cullity, B.D.; Graham, C.D. *Introduction to Magnetic Materials*, 2nd ed.; Wiley-IEEE Press: New York, NY, USA, 2009; ISBN 978-0-471-47741-9.
19. Walther, F. Microstructure-oriented fatigue assessment of construction materials and joints using short-time load increase procedure. *Mater. Test* **2014**, *56*, 519–527. [[CrossRef](#)]
20. Wittkop, S. Einlippentiefbohren Nichtrostender Stähle. Ph.D. Thesis, TU Dortmund, Dortmund, Germany, 11 January 2007.
21. Biermann, D.; Heilmann, M.; Kirschner, M. Analysis of the influence of tool geometry on surface integrity in single-lip deep hole drilling with small diameters. *Procedia Eng.* **2011**, *19*, 16–21. [[CrossRef](#)]
22. Nickel, J.; Baak, N.; Biermann, D.; Walther, F. Influence of the deep hole drilling process and sulphur content on the fatigue strength of AISI 4140 steel components. *Proc. CIRP* **2018**, *71*, 209–214. [[CrossRef](#)]
23. Manns, T. Analyse Oberflächennaher Eigenspannungszustände Mittels Komplementärer Beugungs-Verfahren. Ph.D. Thesis, Universität Kassel, Kassel, Germany, 2010.
24. Timmermann, K. Zur Schädigungsentwicklung bei der Korrosionsermüdung von Aluminium basislegierungen mit Definierten Fertigungsbedingten Randschichtzuständen. Ph.D. Thesis, Universität Kassel, Kassel, Germany.
25. Novovic, D.; Dewes, R.C.; Aspinwall, D.K.; Voice, W.; Bowen, P. The effect of machined topography and integrity on fatigue life. *Int. J. Mach. Tools Manuf.* **2004**, *44*, 125–134. [[CrossRef](#)]
26. Baak, N.; Nickel, J.; Biermann, D.; Walther, F. Micromagnetic-based fatigue life prediction of single-lip deep drilled AISI 4140. In Proceedings of the XIX International Colloquium on Mechanical Fatigue of Metals, Porto, Portugal, 5–7 September 2018; Springer: Cham, Germany, 2018.



© 2018 by the authors. Licensee MDPI, Basel, Switzerland. This article is an open access article distributed under the terms and conditions of the Creative Commons Attribution (CC BY) license (<http://creativecommons.org/licenses/by/4.0/>).